The vacuum-ultraviolet photoelectron spectra of CH_2F_2 and CH_2Cl_2 revisited

Tuckett, Richard; Harvey, Jonelle; Hemberger, Patrick; Bodi, Andras

DOI:
10.1016/j.jms.2015.02.012

Journal of Molecular Spectroscopy 315 (2015) 172–183

Contents lists available at ScienceDirect

Journal of Molecular Spectroscopy

journal homepage: www.elsevier.com/locate/jms

The vacuum-ultraviolet photoelectron spectra of CH_2F_2 and CH_2Cl_2 revisited

Richard Tuckett [a,*], Jonelle Harvey [a,1], Patrick Hemberger [b], Andras Bodi [b]

[a] School of Chemistry, University of Birmingham, Edgbaston, Birmingham B15 2TT, UK
[b] Molecular Dynamics Group, Paul Scherrer Institut, CH-5232 Villigen, Switzerland

ARTICLE INFO

Article history:
Received 24 January 2015
In revised form 18 February 2015
Available online 3 March 2015

Keywords:
Threshold photoelectron spectroscopy
Synchrotron radiation
Methylene fluoride
Methylene chloride
Ionisation energy
Vibrational modes
iPEPICO

ABSTRACT

The threshold photoelectron spectrum (TPES) of difluoromethane and dichloromethane has been recorded at the Swiss Light Source with a resolution of 2 meV or 16 cm^{-1}. Electronic and vibronic transitions are simulated and assigned with the help of Franck–Condon (FC) calculations based on coupled cluster electronic structure calculations for the equilibrium geometries and harmonic vibrational frequencies of the neutrals, and of the ground and excited electronic states of the cations. Notwithstanding a high-resolution pulsed-field ionisation study on CH_2F_2 (Forysinski et al., 2010) in which a number of transitions to the $\tilde{X}^+$ state have been recorded with unprecedented accuracy, we report the first complete vibrationally resolved overview of the low-lying electronic states of $CH_2X_2^+$, X = F or Cl. Hydrogen atom loss from $CH_2F_2^+$ occurs at low energy, making the ground state rather anharmonic and interpretation of the $\tilde{X}^+$ band challenging in the harmonic approximation. By Franck–Condon fits, the adiabatic ionisation energies to the $\tilde{A}^+\ ^2B_2$, $\tilde{C}^+\ ^2A_2$ and $\tilde{D}^+\ ^2B_2$ states have been determined as 14.3 ± 0.1, 15.57 ± 0.01 and 18.0 ± 0.1 eV, respectively. The first band in the CH_2Cl_2 TPES is complex for a different reason, as it is the result of two overlapping ionic states, $\tilde{X}^+\ ^2B_2$ and $\tilde{A}^+\ ^2B_1$, with derived ionisation energies of 11.0 ± 0.2 and 11.317 ± 0.006 eV, and dominated by an extended progression in the CCl_2 bend (in $\tilde{X}^+$) and a short progression in the CCl_2 symmetric stretch (in $\tilde{A}^+$), respectively. Furthermore, even though Koopmans' approximation holds for the vertical ionisations, the $\tilde{X}^+$ state of $CH_2Cl_2^+$ is stabilized by geometry relaxation and corresponds to ionisation from the (HOMO−1) orbital. That is, the first two *vertical* ionisation energies are in the same order as the negative of the orbital energies of the highest occupied orbitals, but the *adiabatic* ionisation energy corresponding to electron removal from the (HOMO−1) is lower than the adiabatic ionisation energy corresponding to electron removal from the HOMO. The second band in the spectrum could be analysed to identify the vibrational progressions and determine adiabatic ionisation energies of 12.15 and 12.25 eV for the $\tilde{B}^+\ ^2A_1$ and $\tilde{C}^+\ ^2A_2$ states. A comparison of the assignment of electronic states with the literature is made difficult by the fact that the B_1 and B_2 irreducible representations in C_{2v} symmetry depend on the principal plane, *i.e.* whether the CX_2 moiety is in the *xz* or the *yz* plane, which is often undefined in older papers.

1. Introduction

Gas-phase vacuum ultraviolet photoelectron spectroscopy, established in the late 1960s, is now a mature technique for determining ionisation energies of molecules and studying their electronic structure. Koopmans' theorem establishes a direct connection between the ionisation energies and the orbital energies in the neutral [1]. The resolution of the technique has improved by orders of magnitude for select systems [2,3], in which pulsed field ionisation with small bandwidth lasers is possible and the spectra can be rovibrationally resolved. Threshold photoelectron detection using velocity map imaging, the approach pursued here [4], allows us to study larger molecules routinely with a few meV, *i.e.* vibrational resolution. In tandem with experimental improvements, transitions can now often be assigned with the aid of *ab initio* calculations, in particular with Franck–Condon (FC) simulations of the vibrational progressions in each cationic electronic state. These advances have led to surprises in the interpretation of the vacuum-UV photoelectron spectra of difluoromethane (CH_2F_2) and dichloromethane (CH_2Cl_2), especially in their ground-state bands, but for different reasons. The purpose

* Corresponding author. Fax: +44 121 414 4403.
E-mail address: r.p.tuckett@bham.ac.uk (R. Tuckett).
[1] Current address: Royal Society of Chemistry, Thomas Graham House, Milton Road, Cambridge CB4 0WF, UK.

http://dx.doi.org/10.1016/j.jms.2015.02.012
0022-2852/

of this paper is to track the history of these spectra since the early days of photoelectron spectroscopy. We show how improvements in both experimental techniques, primarily in the resolution of photon sources and modern electron analysers, and *ab initio* theoretical methods have led to a deeper understanding of these deceptively simple-looking spectra. Certainly for CH_2F_2, the apparent clarity of a single progression in the $\widetilde{X}^+$ band, as first observed over forty years ago by several groups [5–7], hides a complex overlap of different vibrational modes in which the effects of anharmonicity are pronounced.

A further and unexpected complication was found to be the assignment of electronic states. Computational chemistry programs rotate molecules in a "standard orientation". This is a deceiving term, since the principal plane, *i.e.* the one spanned by the three heavy atoms in the molecule, is sometimes defined as the *xz*, sometimes as the *yz* plane in widely-used computer programs. If the molecule is rotated from one orientation to the other, electronic and vibronic states belonging to the irreducible representations B_1 and B_2 are swapped. While it is conceptually easy to find the irreducible representation of a vibrational mode with a description in any convention, molecular orbitals (MOs) are rarely described in detail. Additionally, some of the MO energies, particularly that of the highest occupied MO (HOMO) and the (HOMO−1) orbital in CH_2Cl_2, are closely spaced and their ordering can be method dependent. Thus, there is no unambiguous way to identify the orientation of the molecule unless it is explicitly given. Herein, we use *yz* as the principal plane, as this is how most computational works have been carried out.

The geometries of neutral CH_2F_2 and CH_2Cl_2 are well established by microwave spectroscopy and related techniques [8,9]; equilibrium values are quoted in Tables 1 and 2 which are invariant to the isotopologue under consideration. Both molecules have nine vibrational modes. Four belong to the a_1 irreducible representation (ν_1 CH_2 symmetric stretch, ν_2 CH_2 bend, ν_3 CX_2 symmetric stretch, ν_4 CX_2 bend), one to a_2 (ν_5 CH_2 twist), two to b_1 (ν_6 CH_2 asymmetric stretch, ν_7 CH_2 rock), and two to b_2 (ν_8 CH_2 wag, ν_9 CX_2 asymmetric stretch). The Mulliken convention is used: the molecule's vibrational modes of the same symmetry are labelled so that the highest-energy vibration belonging to the a_1 irreducible representation is ν_1, the second highest is ν_2, *etc.* Two a_1 symmetry modes in CH_2F_2, the CH_2 bend and CF_2 symmetric stretch, as well as the two b_2 modes, the CH_2 wag and CF_2 asymmetric stretch, have a different ordering in the $\widetilde{X}^+$ electronic ground state of the cation. For consistency, and in order to have a compact way of denoting sequence and hot bands, we maintain the above labelling unchanged for $CH_2F_2^+$. Thus the ν_2^+ mode of $\widetilde{X}^+$ $CH_2F_2^+$ continues to describe the CH_2 bending mode, even though the ν_3^+ mode describing the CF_2 symmetric stretch has a *higher* frequency. Likewise, the eighth mode of the ground-state cation is used to describe the CH_2 wag and the ninth mode the CF_2 asymmetric stretch, even though $\nu_8^+ < \nu_9^+$. The energetic reversal of these two pairs of vibrational modes arises essentially because of the significant change in geometry and, hence, in the force constants upon ionisation in CH_2F_2, and has caused confusion and misunderstandings in previous papers.

Following high-resolution Fourier transform infrared (IR) measurements by Smith et al. [10,11], Deo et al. [12,13], and Cronin et al. [14] including decoupling of the multiple Coriolis interactions between ν_2 and ν_8, ν_3 and ν_9, ν_5 and ν_7, and ν_6 and $2\nu_2$, the experimental values of the nine vibrational fundamentals in CH_2F_2 are well established and listed in Table 1. It is, thus, not surprising that the first photoelectron band corresponding to $\widetilde{X}^+$ $CH_2F_2^+$ is complicated on spectroscopic grounds alone because Coriolis interactions are prevalent in the neutral, making formally-forbidden IR transitions, such as ν_5 (a_2), observable. In this context, it would be surprising if only a simple progression of totally symmetric a_1 vibrations were observed in the photoelectron spectrum.

Numerous geometry optimizations and normal mode analyses have been reported for both CH_2F_2 and its parent cation, with improving accuracy with increased basis set size and more rigorous description of electron correlation up to coupled cluster CCSD(T) theory [15–18]. However, most calculations on the neutral molecule have been made in the harmonic approximation with no interaction between the nine normal modes. The recent paper of Luckhaus et al. [19] allows for fully coupled anharmonic effects and Coriolis or Fermi interactions between close-lying vibrational levels, and the results are impressive; for the neutral molecule most calculated vibrational transitions lie within 2 cm^{-1} of the experimental data, with a maximum deviation of only 3 cm^{-1}. Data for the harmonic vibrational frequencies of the ground state of $CH_2F_2^+$ have been reported at different levels of theory by Takeshita and Forysinski et al. [15,18]. The most significant points to note from both studies are that the a_1 vibration describing the CF_2 symmetric stretch vibration (which we label ν_3^+) is of higher energy than the CH_2 bend (ν_2^+), and the eigenvalue for the CF_2 asymmetric stretch (ν_9^+ of b_2 symmetry) exceeds that of the CH_2 wag (ν_8^+ in our notation). The changes in vibrational levels correlate with the calculated geometry change upon ionisation; an increase in C–H bond length (ΔR_e = +0.09 Å), a decrease in C–F length (ΔR_e = −0.09 Å), an 8° increase in the FCF bond angle, and a large, 27° decrease in the HCH angle. The attempts of Luckhaus et al. to apply their methodology to the ground state of the open-shell cation $CH_2F_2^+$ are also revealing [19]. Very few of the lowest-lying vibrational levels can be described as 'pure,' and the effects of anharmonicity are pronounced even at modest levels of vibrational excitation above the zero-point energy level. The situation is complicated, or perhaps partially explained, by the fact that the lowest dissociation threshold to $CHF_2^+ + H$ lies only 2740 cm^{-1} above the $v^+ = 0$ level [18,20], so the electronic potential of $\widetilde{X}^+$ $CH_2F_2^+$ only supports few bound states. This energy is also close to the FC maximum of the ground state of $CH_2F_2^+$, and significant anharmonic effects are therefore expected in the excitation of any of the nine vibrational fundamental modes. It is therefore predicted that attempts to analyse higher-resolution photoelectron spectra of the first band of CH_2F_2 will encounter problems if the conventional, harmonic approach is taken. This has already been appreciated by Forysinski et al. in their attempt to analyse the pulsed field ionisation zero kinetic energy (PFI-ZEKE) photoelectron spectrum of CH_2F_2 recorded at a superb, 1 cm^{-1} resolution [18]. As will be seen later in the FC simulations, anharmonic effects are by far the most pronounced in the vibrational structure of the ground state of $CH_2F_2^+$. In fact, even in $CH_2F_2^+$, the vibrational transitions are not defined or resolved well enough to warrant an anharmonic analysis at our spectral resolution. Instead, we analyse all vibrational fine structure in the harmonic approximation but refer the reader to Luckhaus et al. [19] for a more accurate analysis of the vibrational states in $\widetilde{X}^+$ $CH_2F_2^+$.

Coriolis interactions are, of course, also prevalent in the IR and Raman spectra of neutral dichloromethane [21–25], and it would therefore be surprising if such effects were not observed in the parent cation. However, the significant difference from difluoromethane is that the first dissociative ionisation threshold from CH_2Cl_2 corresponds not to H-atom loss, but to Cl-atom loss and at a much higher energy above the adiabatic ionisation energy (IE). In the so far highest-resolution (*ca.* 0.002 eV or 16 cm^{-1}) study of this process, we determined the dissociation threshold to $CH_2Cl^+ + Cl$ to be 12.108 ± 0.003 eV [20], which is 0.791 eV (or 6380 cm^{-1}) above the experimental adiabatic IE of the $\widetilde{A}^+ {}^2B_1$ state of $CH_2Cl_2^+$. Due to the large geometry relaxation, the origin of the

Table 1
Experimental and *ab initio* vibrational frequencies, and geometries of CH_2F_2. Vibrational frequencies in cm^{-1}, bond lengths in Å, bond angles in degrees (°).

Mode	Description	$\tilde{X}\ ^1A_1$		$\tilde{X}^+\ ^2B_1$	$\tilde{A}^+\ ^2B_2$	$\tilde{B}^+\ ^2A_1$	$\tilde{C}^+\ ^2A_2$	$\tilde{D}^+\ ^2B_2$	$\tilde{E}^+\ ^2A_1$	$\tilde{F}^+\ ^2B_1$
		expt[a]	CCSD/cc-pVTZ[b]	EOM-IP-CCSD/cc-pVTZ[b]						
ν_1 (a_1)	CH_2 sym-stretch	2948.0	3100	2548	3182	2806	3162	3151	2931	2967
ν_2 (a_1)	CH_2 bend	1509.1	1573	1092	1526	1418	1524	1454	1368	1550
ν_3 (a_1)	CF_2 sym-stretch	1111.6	1162	1290	1116	907	1027	851	854	1023
ν_4 (a_1)	CF_2 bend	528.5	546	608	540	455	480	434	364	459
ν_5 (a_2)	CH_2 twist	1255.8	1309	1011	1114	1178	1159	787	1207	imag
ν_6 (b_1)	CH_2 asym-stretch	3014.0	3170	2124	3331	3307	3296	3310	3022	1643
ν_7 (b_1)	CH_2 rock	1178.6	1216	580	1182	1369	1165	1060	973	793
ν_8 (b_2)	CH_2 wag	1435.6	1501	1103	1348	1282	1721	1070	1320	1189
ν_9 (b_2)	CF_2 asym-stretch	1090.1	1167	1508	432	imag	646	610	imag	1657
R_e (C–H)		1.084	1.088	1.169	1.081	1.111	1.083	1.085	1.102	1.150
R_e (C–F)		1.351	1.350	1.269	1.405	1.367	1.421	1.505	1.499	1.436
$\langle HCH\rangle_e$		112.8	112.8	86.2	122.5	126.1	120.1	123.9	137.9	99.0
$\langle FCF\rangle_e$		108.5	108.6	116.7	83.8	117.9	97.4	93.6	112.7	107.0
$\langle HCF\rangle_e$			108.8	112.5	111.0	103.5	109.2	108.8	101.5	112.7

[a] Refs. [8,10–14].
[b] This work.

Table 2
Experimental and *ab initio* vibrational frequencies, and geometries of CH_2Cl_2. Vibrational frequencies in cm^{-1}, bond lengths in Å, bond angles in degrees (°).

Mode	Description	$\tilde{X}\ ^1A_1$		$\tilde{X}^+\ ^2B_2$	$\tilde{A}^+\ ^2B_1$	$\tilde{B}^+\ ^2A_1$	$\tilde{C}^+\ ^2A_2$
		expt[a]	CCSD/cc-pVTZ[b]	EOM-IP-CCSD/cc-pVTZ[b]			
ν_1 (a_1)	CH_2 sym-stretch	2997.7	3153	3164	2880	3024	3148
ν_2 (a_1)	CH_2 bend	1435.0	1492	1475	1163	1403	1477
ν_3 (a_1)	CCl_2 sym-stretch	714.5	734	789	701	616	710
ν_4 (a_1)	CCl_2 bend	281.5	288	304	316	287	272
ν_5 (a_2)	CH_2 twist	1153.0	1198	1084	1002	1145	1150
ν_6 (b_1)	CH_2 asym-stretch	3053.0	3228	3279	2811	3289	3247
ν_7 (b_1)	CH_2 rock	898.7	918	966	331	1129	935
ν_8 (b_2)	CH_2 wag	1268.9	1313	1241	982	2072	1764
ν_9 (b_2)	CCl_2 asym-stretch	757.7	796	624	849	866	693
R_e(C–H)		1.080	1.082	1.082	1.112	1.093	1.083
R_e(C–Cl)		1.766	1.773	1.781	1.716	1.770	1.800
$\langle HCH\rangle_e$		112.1	111.5	117.4	102.5	118.1	114.3
$\langle ClCCl\rangle_e$		112.0	112.6	90.3	119.1	122.1	105.0
$\langle HCCl\rangle_e$			108.2	111.5	108.5	104.4	109.3

[a] Refs. [9,21–25].
[b] This work.

$(7b_2)^{-1}$ ionisation to the $\tilde{X}^+\ ^2B_2$ state of $CH_2Cl_2^+$ lies even lower. Not only are these bond dissociation energies significantly larger than their equivalent in $CH_2F_2^+$, but they also mean that the first dissociative ionisation threshold lies well above the FC envelope of $\tilde{X}^+$ $CH_2Cl_2^+$. The anharmonic effects on the vibrational fine structure in the first photoelectron band of CH_2Cl_2 are therefore less pronounced. The experimental and calculated geometries of CH_2Cl_2 and its cation are shown in Table 2 [9,26,27]. Perhaps the most significant point to appreciate is that the origin transition in unlikely to be observed for the $\tilde{X}^+$ state because of the large decrease in ClCCl bond angle of 22°; the C–H and C–Cl bond lengths are virtually unchanged and the HCH bond angle increases by only 5°. Thus, to a first approximation, one expects the greatest FC activity in the $\tilde{X}^+$ photoelectron band of CH_2Cl_2 to be seen in the ν_4 CCl_2 bending mode, *not* in the ν_2 CH_2 bending mode as in the corresponding $\tilde{X}^+\ ^2B_1$ state of $CH_2F_2^+$ where the HCH bond angle is calculated to decrease significantly upon ionisation by 26°.

In this paper, we report the valence vacuum-UV threshold photoelectron spectrum of CH_2F_2 and CH_2Cl_2 recorded at the 3rd generation Swiss Synchrotron Light Source, SLS, from their ionisation onset, 11–12 eV, to 20 and 16 eV, respectively. The resolution of the spectra is *ca.* 0.002 eV or 16 cm^{-1}. Photoions were also recorded in coincidence, and the results of this dynamical fragmentation study and of earlier studies using a 2nd generation synchrotron are published elsewhere [20,28,29]. We analyse the threshold photoelectron spectra in the light of new *ab initio* calculations and Franck–Condon simulations, and reflect on how the interpretation of these apparently simple spectra has evolved over the years.

2. Experimental and theoretical methods

The imaging photoelectron photoion coincidence (*i*PEPICO) spectrometer at the X04DB vacuum ultraviolet beamline of the SLS has been described in detail elsewhere [30,31]. Pure sample is introduced into the chamber through an effusive source at room temperature. Typical pressure in the experimental chamber was 2–4 × 10^{-6} mbar, against a background pressure of 1 × 10^{-7} mbar. The sample is ionised by monochromatic VUV radiation dispersed by a grazing incidence monochromator. Two gratings are available, interchangeable under vacuum, with maximum output at 12 eV (600 lines mm^{-1}) and 20 eV (1200 lines mm^{-1}). The optimum photon resolution is *ca.* 0.002 eV. The photon energy is calibrated against autoionisation lines of argon and neon in first and second order. Higher orders of radiation are removed using a compact gas filter with an absorption path length of 10 cm and operating at 10 mbar of Ne.

Photoelectrons are extracted by a 120 V cm^{-1} continuous field and velocity map imaged onto a position sensitive delay line anode (Roentdek DLD40) with a kinetic energy resolution of 1 meV at threshold. 'Hot' electrons with non-zero kinetic energy can have a velocity vector that is oriented along the flight tube axis. If so, they also arrive at the centre of the detector along with the threshold electrons, and can be removed by a subtraction technique [32]. The resulting spectra are flux normalised using a sodium salicylate coated pyrex window with a visible photomultiplier tube. We have already established that the TPES peak positions of a range of fluoroethene molecules were not Stark shifted measurably in an extraction field as high as 120 V cm^{-1} [33], and assume the same applies to the molecules studied herein. However, we note that peak positions may be shifted to lower energy by as much as 8 meV, in the unlikely event that this assumption is incorrect [34]. The uncertainties for both the adiabatic and vertical IEs were determined from the half width at half maximum of a Gaussian function fitted to the experimental spectrum when the corresponding origin transition was detected. When extrapolating to the onset of a progression with a 0–0 vibrational transition of negligible intensity, we estimated the uncertainty in the number of vibrational quanta at the detected transitions and have set the error bar accordingly.

$CH_2F_2(g)$ and $CH_2Cl_2(l)$ samples were obtained from Fluorochem UK (99.9%) and Aldrich Chemical Company, respectively. The former was used without purification, the latter was subject to several freeze-pump-thaw cycles before introduction in the experimental chamber.

The geometry of the neutral ground electronic state of both CH_2F_2 and CH_2Cl_2 was optimised and the numerical frequency analysis was carried out employing coupled cluster theory with singles and doubles (CCSD) in the frozen core approximation with the cc-pVTZ basis set using Q-Chem 4.0.1 [35]. For the electronic ground and excited cationic states, we used the equation-of-motion for ionisation potential (EOM-IP-)CCSD approach with the said basis set. The frequency analyses confirmed the stationary points to be minima unless noted otherwise, and the computed Hessian matrices were used in FC calculations. We note that Q-Chem uses the *xz* principal plane as opposed to our choice of the *yz* principal plane in C_{2v} symmetry. Irreducible representations given for electronic states and normal modes listed herein are correct when the molecule is oriented so that the CX_2 moiety is in the *yz* plane.

Franck–Condon simulations were performed with the program eZspectrum.OSX [36], based on the optimised geometries and force constants of the contributing states. Unscaled frequencies were used, and the Dushinsky rotation was taken into account. All spectra were simulated at room temperature and the phase space of the fit, defined by the excitation space of both neutrals and ions, was successively increased until the spectrum did not change significantly. Resulting stick spectra were subsequently convoluted with a Gaussian function to match the experimental spectrum. When the photoelectron band is comprised of excitations into two or more different electronic ion states, separate simulations were performed, which were then convoluted, weighted, and summed to fit the observed band system.

3. Results and discussion

3.1. Difluoromethane, CH_2F_2

The threshold photoelectron spectrum of CH_2F_2 between 12.7 and 20.5 eV is shown in Fig. 1, recorded at a resolution of 0.006 eV, along with calculated adiabatic ionisation energies at the EOM-IP-CCSD/cc-pVTZ level of theory. This spectrum is a composite between two scans recorded with the lower-energy grating (up to 13.7 eV) and the higher-energy grating (above 13.7 eV). A significant overlap between the two scans ensures the validity of the relative intensities of the different photoelectron bands. A new spectrum of the first photoelectron band between 12.7 and 13.8 eV with improved resolution, 0.002 eV, and longer signal averaging is shown in Fig. 2.

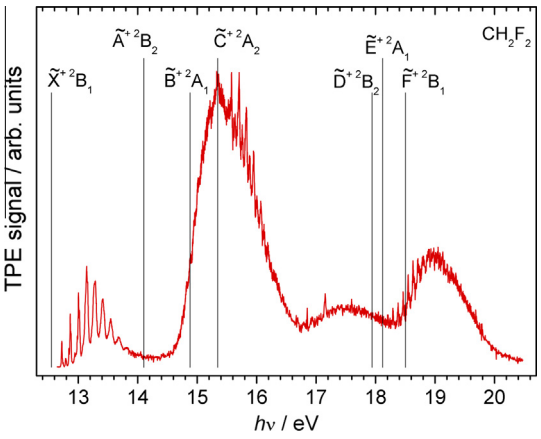

Fig. 1. Threshold photoelectron spectrum of CH_2F_2 in the 12.7–20.5 eV photon energy range recorded with a step size of 0.006 eV and an integration time of 30 s per point. The spectrum has been flux normalised, and is a composite of two spectra; one recorded below 13.7 eV with the lower-energy grating, and one above 13.7 eV with the high-energy grating. Vertical lines indicate adiabatic ionisation energies calculated at the EOM-IP-CCSD/cc-pVTZ level of theory.

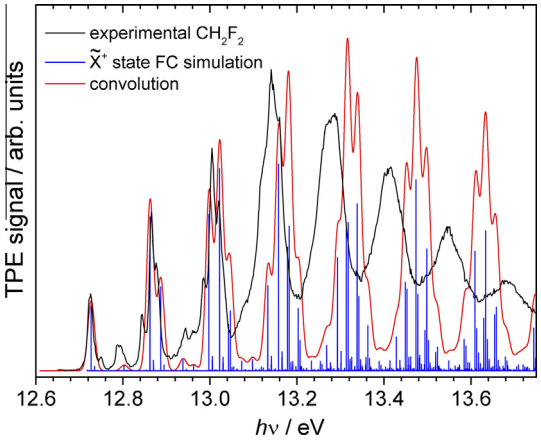

Fig. 2. The first photoelectron band of CH_2F_2 (ionisation to $CH_2F_2^+$ $\tilde{X}^{+\,2}B_1$) recorded between 12.65 and 13.85 eV with a step size of 0.002 eV and an integration time of 90 s per point. The spectrum has been flux normalised. A Franck–Condon simulation (blue sticks) and convolution with a Gaussian function (FWHM = 18 meV) to account for unresolved rotational structure (red) are also shown.

The ordering of the outer CH_2F_2 Hartree–Fock molecular orbitals (MO) using the cc-pVTZ basis set and the *yz* principal plane is $\ldots(1b_1)^2(5a_1)^2(3b_2)^2(1a_2)^2(4b_2)^2(6a_1)^2(2b_1)^2$, where the orbital numbering includes the C and F 1s core orbitals. The $4b_2$ and $6a_1$ orbitals lie close in energy and are exchanged in density functional theory results, which shows that there is no unambiguous ordering of the MOs in this molecule [6,15]. Pullen et al. report a $^2B_1$ ground ion state [7], whereas Brundle et al. propose it to be of $^2B_2$ symmetry [6], which could indicate that they were working in different coordinate systems but identified the correct ground state. However, probably because of the limited computational possibilities at the time, they could not identify the following three states correctly. The HOMO of $2b_1$ symmetry has C–H bonding and C–F antibonding character. Both vertical and adiabatic ionisation energy calculations confirm that the lowest lying cationic electronic state is indeed $\tilde{X}^{+\,2}B_1$, thus corresponding to electron

removal from the HOMO, which leads to a lengthening of the C–H and a shortening of the C–F bond (Table 1). In the harmonic approximation, Franck–Condon activity should only be observed in vibrational modes of $CH_2F_2^+$ (of either fundamental, overtone or combination bands) with a_1 symmetry or with even quanta in non-totally symmetric normal modes. Band positions are tabulated in Table 3, and compared with the recent PFI-ZEKE data of Forysinski et al. [18] and earlier photoelectron studies using fixed-energy lamp sources or low-resolution synchrotron studies [28,37]. At first sight, the appearance of our spectrum looks very similar to the earlier lower-resolution studies, with a progression being observed in a mode with a FC maximum around $v_i = 3$. However, at our resolution of *ca.* 0.002 eV the peaks with $v_i = 1$, 2 or 3 are clear doublets, and the higher peaks in this progression are significantly broadened. In addition, there is clear vibrational activity observed between the band origin at 12.727 eV and $v_i = 1$, between $v_i = 1$ and $v_i = 2$, and possibly between $v_i = 2$ and $v_i = 3$. Apart from the peak broadening, this intermediate structure is lost after $v_i = 3$ at 13.142 eV. No hot band structure is observed below 12.727 eV, which is somewhat surprising as the lowest-energy a_1 mode ($\nu_4 = 529\ cm^{-1}$) should have measurable population in its lower levels (certainly in $v = 1$) at the temperature of the experiment, 298 K.

The history of the assignment of this band when recorded with inferior resolution, *ca.* 0.03 eV, is interesting. From the first photoelectron spectra, Potts et al. [5] assigned the 'single progression' to the CH_2 bending mode and obtained $\nu_2^+ = 1120\ cm^{-1}$. Brundle et al. [6] agreed with this assignment and obtained $\nu_2^+ = 1010\ cm^{-1}$, but thought it likely that another overlapping and almost degenerate vibrational progression, presumably of a_1 symmetry, too, was also present, because vibrational structure was lost for CD_2F_2; this indicated that the vibrational structure in CH_2F_2 did not correspond to a single vibrational mode. Pullen et al. [7] thought the single band could be a complicated overlap of the CF_2 symmetric stretch, the CH_2 twist, the CH_2 rock and the CF_2 asymmetric stretch, although it is not clear whether they appreciated that the last three modes do not have a_1 symmetry and odd-quantum transitions are therefore formally forbidden in photoelectron spectroscopy. None of these early studies from the 1970s had the advantage of modern *ab initio* packages to aid in the assignment. In 1990, Takeshita first performed geometry and vibrational frequency calculations both on neutral CH_2F_2 and the first four electronic states of $CH_2F_2^+$ in C_{2v} symmetry, *i.e.* its ground state and the three lowest excited states, using self-consistent field methods and the *xz* convention for the principal plane [15]. Calculations were made in the harmonic approximation, only a_1 progressions were therefore considered, and Franck–Condon simulations were attempted. He assigned the single progression to an overlap of three modes, ν_1^+, ν_2^+ and ν_3^+, with the apparent single progression arising because two of the vibrational wavenumbers are similar and half the value of the third, *i.e.* $\nu_2^+ \approx \nu_3^+ \approx \frac{1}{2}\nu_1^+$. The FC simulation predicted a long progression in the 'single' vibrational progression, peaking at $v_i \approx 7$ and extending to beyond $v_i \approx 14$. However, as noted by Takeshita, under non-resonant HeI (21.22 eV) excitation, the maximum observed transition is at $v_i \approx 3$. In 1993, Pradeep and Shirley also recorded the HeI photoelectron spectrum of cold CH_2F_2 under supersonic beam conditions and an improved resolution of 0.013 eV, identifying the ionic ground state as $^2B_2$ and therefore implying an *xz* principal plane [37]. They believed they could resolve three independent but overlapping progressions which they assigned to the symmetric vibrations ν_2^+, ν_3^+ and $2\nu_4^+$, although no attempt was made to explain why progressions only involving even quanta of ν_4^+ were observed. In 2001, the band was recorded by Seccombe et al. under threshold conditions for the first time using tunable vacuum UV radiation from a 2nd generation synchrotron and term symbols are reported using the *xz* convention [28]. However, the modest resolution of the beamline, *ca.* 0.015 eV, meant that no new information was obtained, and the single progression observed was assigned to overlapping progressions in the CH_2 stretch, ν_2^+, and the CF_2 symmetric stretch, ν_3^+, with an average value of $1130\ cm^{-1}$. An extra peak between the origin band and $v_i = 1$ was observed at *ca.* 12.8 eV, but was not assigned. As in the HeI studies, the maximum in the band was also observed at $v_i \approx 3$.

We have performed independent FC calculations in the harmonic approximation and simulated the vibrational structure of the first photoelectron band of CH_2F_2, using optimised geometries and Hessian matrices obtained at the (EOM-IP-)CCSD/cc-pVTZ level of theory. The geometries and vibrational frequencies calculated for the neutral and ground state of the cation are given in Table 1. The energies of the predicted bands, their relative FC factors and their assignments are given in Table S1 of the Supplementary Material. Fig. 2 shows our experimental spectrum (black[2]), a stick spectrum of the vibrational bands with significant FC activity (blue), and a convolution of the predicted bands with a Gaussian function with full width at half maximum, FWHM, of 18 meV to account for the unresolved rotational structure (red). The adiabatic IE of the simulated spectrum is set to the same value as our experimental value, 12.727 eV. The assignments of the peaks are given in Table 3. The agreement with experiment is much better than that reported by Takeshita [15] in that the simulation predicts a maximum at $v_i = 3$–4, in agreement with experiment. As expected, the effects of anharmonicity in the experimental spectrum become more pronounced as the energy increases, and there are a number of unassigned peaks near the adiabatic IE. Since these calculations are performed in the harmonic approximation, all assignments only involve vibrational modes in the cation of a_1 symmetry (ν_1^+ through ν_4^+) or even combinations of non-symmetric vibrations (*e.g.* $2\nu_7^+$).

A major change in understanding of this band came in 2010, when Forysinski et al. applied PFI-ZEKE spectroscopy using a vacuum-UV laser to record the spectrum at a resolution of *ca.* $1\ cm^{-1}$, *i.e.* at least two orders of magnitude better than in previous studies. They reported the band origin for ionisation to $\widetilde{X}^+\ CH_2F_2^+$ to be $102\,636 \pm 7\ cm^{-1}$ (12.7252 ± 0.0009 eV) [18]. Furthermore, they observed that the 'single' peaks around 1100 and $2200\ cm^{-1}$ to higher energy were in fact a triplet and, possibly, a quintet of peaks, respectively, with weak structure in between. The spectrum was not recorded between the origin band and the triplet of lines at *ca.* $1100\ cm^{-1}$, or at energies above the dissociative ionisation threshold to $CHF_2^+ + H$ of $105\,375 \pm 25\ cm^{-1}$ (13.065 ± 0.003 eV). As seen in Fig. 2, there is in fact significant threshold photoelectron signal in both these ranges. The explanation of the absence of the second set of peaks is most likely that fragmentation of the Rydberg states above this dissociative ionisation threshold is so fast that the bands are broadened considerably and the ZEKE signal falls below the detection limit.

The line positions of the bands observed by Forysinski et al. are shown in Table 3. They concluded that their spectrum could not be fully assigned unless anharmonic contributions from all vibrational modes were accounted for. The results of the fully-coupled anharmonic calculations for the ground electronic states of CH_2F_2 and $CH_2F_2^+$ were published later in the same year by Luckhaus et al. [19]. Whilst the calculations were relatively easy to converge for the closed-shell $\widetilde{X}\ CH_2F_2$ molecule, there were more difficulties for the open-shell $\widetilde{X}^+\ CH_2F_2^+$ species. Nevertheless, they were able to assign most of the strong transitions observed in the PFI-ZEKE spectrum to a_1 vibrations or overtones and combination bands of a_1 symmetry, the energies and relative intensities also being shown

[2] For interpretation of color in Figs. 2 and 7, the reader is referred to the web version of this article.

Table 3
Energies (eV) of vibrational bands observed in the vacuum-UV photoelectron spectrum of CH_2F_2 and comparison with earlier data.

hν (eV)	Separation		Comment	FC	Forysinski 2010[a]		Luckhaus 2010[b]			Pradeep 1993[c]		Seccombe 2001[d]	
	(meV)	(cm^{-1})		Simulation	Energy (eV)	Comment	Assignment (% leading terms)		Rel. intensity				
12.727			AIE	0_0^0	12.725_2	0_0^0	12.725_2[e]	0_0^0 (92)	4.2	12.729	0_0^0	12.74	0_0^0
12.748	21	169	Very weak	4_1^1									
12.792	65	524	Broad	4_0^1			12.799_2	4_0^1 (92)	0.4				
12.844	117	944	Medium	–	12.845_3	Strong	12.844_1	2_0^1 (49), 7_0^2 (32)	7.0	12.859	4_0^2		
12.865	138	1113	Strong	2_0^1	12.866_2	Strong	12.865_4	2_0^1 (40), 7_0^2 (45)	5.7	12.872	2_0^1	12.88	2_0^1 or 3_0^1
12.876	149	1202	Shoulder	3_0^1	12.879_7	Strong	12.880_3	3_0^1 (82),	6.8	12.874	3_0^1		
					12.932_1	Medium							
12.944	217	1750		$2_0^1 4_0^1$	12.940_2, 12.944_0, 12.950_5		12.949_5	$2_0^1 7_0^2$ (26), 7_0^4 (10)	3.0				
12.963	236	1903	Shoulder, weak	$3_0^1 4_0^1$	12.958_9 and 12.964_9, all weak		12.965_2	$6_0^1 7_0^1$ (23), 1_0^1 (21)	3.6				
12.986	259	2089	Medium	2_0^2	12.985_6	Strong	12.982_8	2_0^2 (52), 5_0^2 (10)	9.4	12.989	4_0^4		
					12.999_6	Weak shoulder	12.999_6	$2_0^1 3_0^1$ (41), $3_0^1 7_0^2$ (24)	7.2				
13.005	278	2242	Strong	$2_0^1 3_0^1/2_0^1 7_0^2$	13.005_0	Strong	13.004_5	$2_0^1 7_0^2$ (28), 7_0^4 (14)	10.0	13.010	2_0^2	13.02	2_0^2 or 3_0^2
					13.008_0	Medium shoulder							
13.020	293	2363	Shoulder	$1_0^1/3_0^2$	13.022_8	Strong	13.021_3	$3_0^1 7_0^2$ (39), $2_0^1 3_0^1$ (24)	9.1	13.014	3_0^2		
					13.034_0	Medium	13.034_4	3_0^2 (59)	5.1				
13.085	358	2887	Shoulder, weak	$2_0^1 3_0^1 4_0^1$	[No structure observed or calculated above the dissociation threshold to $CHF_2^+ + H$ of *ca.* 13.06 eV]								
13.124	397	3202	Shoulder	2_0^3						13.118	4_0^6		
13.142	415	3347	VIE	$2_0^2 3_0^1$						13.145	2_0^3	13.16	2_0^3 or 3_0^3
13.159	432	3484	Shoulder	$1_0^1 2_0^1/2_0^1 3_0^2$						13.152	3_0^3		
13.274	547	4412	Broad	$2_0^3 3_0^1/1_0^1 2_0^2/2_0^2 3_0^2/1_0^1 2_0^1 3_0^1/$ $2_0^1 3_0^3$						13.278	2_0^4	13.30	2_0^4 or 3_0^4
13.287	560	4516								13.289	3_0^4		
13.401	674	5436	Broad	$1_0^1 2_0^3/1_0^1 2_0^2 3_0^1/1_0^1 2_0^1 3_0^2$						13.407	2_0^5	13.44	2_0^5 or 3_0^5
13.414	687	5541								13.435	3_0^5		
13.547	820	6613	Broad							13.535	2_0^6	13.55	2_0^6 or 3_0^6
										13.560	3_0^6		
13.677	950	7662	Broad							13.660	2_0^7	13.70	2_0^7 or 3_0^7
										13.694	3_0^7		

[a] Ref. [18].
[b] Ref. [19], the numbering of the vibrational modes has been changed so that they conform to our usage.
[c] Ref. [37].
[d] Ref. [28].
[e] Assumed value from [18].

in Table 3. Nearly all the observed bands had contributions from several normal mode basis functions, and no band could be described as a 'pure' transition. This is especially true near the dissociation threshold to $CHF_2^+ + H$, 2740 cm^{-1} above the $v^+ = 0$ level of $\widetilde{X}^+$ $CH_2F_2^+$. Fundamental band transitions (nominally labelled v_5^+ through v_9^+) of a_2, b_1 or b_2 symmetry were calculated to have very low FC intensity, and the authors commented that, far from indicating a breakdown of the FC principle when anharmonic effects are considered, the opposite is, perhaps surprisingly, the truth.

As shown in Table 3, the peak positions from our threshold photoelectron spectrum recorded at a resolution of *ca.* 16 cm^{-1} and those recorded by PFI-ZEKE at a resolution of *ca.* 1 cm^{-1} are in excellent agreement, to within 1–3 meV or 8–24 cm^{-1}, up to the dissociation energy to $CHF_2^+ + H$, 13.06 eV. As noted above, two low-energy bands near the adiabatic IE have not been reported in the PFI-ZEKE spectrum. The band at 12.792 eV, 65 meV or 524 cm^{-1} above the adiabatic IE, is significantly below the first dissociation threshold, and it therefore seems reasonable to believe that the predominant basis function of this band must be due to a vibration of a_1 symmetry. Our FC simulation shows that indeed the $v_4^+ = 1$ transition is populated, although its vibrational frequency is significantly higher at 608 cm^{-1} in our harmonic calculations, compared to 597 cm^{-1} in the anharmonic calculations of Luckhaus et al. [19]. The weak but distinct band at 12.748 eV, 21 meV or 169 cm^{-1} above the adiabatic IE, is probably due to a sequence band from an excited vibrational level of $\widetilde{X}$ $^1A_1$ CH_2F_2. The most likely assignment is $v_3 = 1 \rightarrow v_3^+ = 1$ or the 3_1^1 transition, since the frequency of this vibrational mode is predicted to *increase* by 128 cm^{-1} upon ionisation in the harmonic calculations and will therefore appear to *higher* energy of the adiabatic IE. We note, however, that neither of the 3_1^0 and 4_1^0 transitions is observed in the room temperature spectrum in Fig. 2 *ca.* 1100 and 530 cm^{-1} to the red of the adiabatic IE, respectively. It is also worth noting that weak Franck–Condon activity is also present in the 4_1^1 band but this transition is lower in energy and probably blended into the 0–0 band. The assignments of bands in the photoelectron spectrum *above* the $CHF_2^+ + H$ dissociation threshold are even more ambiguous. Whilst the spectrum appears to simplify and becomes a single progression of broader lines, it is now clear from the calculations of Luckhaus et al. that it is probably an oversimplification to assign these lines to a simple progression in v_2^+, v_3^+, v_4^+, or to some combination thereof [19]. For the sake of completeness, the assignments given to these higher-energy lines both by Seccombe et al. and Pradeep et al. remain in Table 2 [28,37], but they have now been shown probably to be incomplete or even incorrect.

3.2. Dichloromethane, CH_2Cl_2

There have been surprisingly few reports on the photoelectron spectrum of CH_2Cl_2, either under non-resonant HeI ($h\nu$ = 21.22 eV)/HeII ($h\nu$ = 40.8 eV) conditions or under threshold electron conditions. Spectra have been recorded with HeI radiation by Potts et al. [5] and Pradeep and Shirley [37], the latter in a supersonic beam with a resolution of 0.013 eV. The HeII spectrum was reported by von Niessen et al. [38]. Dixon et al. interpreted the first bands of the spectrum of CH_2Cl_2 as ionisation from non-bonding *p* orbitals on the Cl atoms coupling weakly to σ-bonding C–H and C–Cl orbitals [39]. To the best of our knowledge there has only been one threshold photoelectron spectrum reported over the complete valence region at a resolution of *ca.* 0.030 eV by Chim [29], with the ground-state band(s) also being recorded with an improved resolution of 0.011 eV. Calculated symmetries, geometries, and vibrational frequencies of the ground and valence-excited states of $CH_2Cl_2^+$ have been reported most recently by Takeshita and Xi et al. [26,40], with term symbols and orbital symmetries both in the *yz*, *i.e.* our, principal plane convention. Just like CH_2F_2, the orbital ordering in dichloromethane is also somewhat method dependent. However, it is quite similar to that of CH_2F_2, and the outer orbital ordering of the Hartree–Fock MOs in the cc-pVTZ basis set corresponds to $\ldots(2b_1)^2(8a_1)^2(6b_2)^2(2a_2)^2(9a_1)^2(7b_2)^2(3b_1)^2$, where the orbital numbering includes the C and Cl core orbitals. In the Kohn–Sham orbital ordering, $9a_1$ lies below the $2a_2$ orbital. The highest-lying b_2 orbital in CH_2Cl_2 is clearly the (HOMO−1). However, the corresponding $^2B_2$ cation state undergoes significant geometry relaxation, and becomes the ground cationic state to which the origin transition is not detected because of a negligible FC factor. It is important to note that Koopmans' approximation does hold, and the vertical transition to the $^2B_1$ state lies lowest in energy at the neutral geometry (at which the separation of the first two vertical ionisation energies is small, only 0.24 eV), meaning that the first sharp peak in the spectrum corresponds to the origin transition to the $\widetilde{A}^+$ state. That is, the vertical ionisation energy to the $\widetilde{X}^+$ state lies *above* the vertical energy to the $\widetilde{A}^+$ state, even though the adiabatic ionisation energy to $\widetilde{X}^+$ lies *below* the adiabatic energy to $\widetilde{A}^+$. Consequently, in contrast with $CH_2F_2^+$ where they are well separated, the FC envelopes of the $\widetilde{X}^+$ $^2B_2$ and $\widetilde{A}^+$ $^2B_1$ bands overlap strongly in $CH_2Cl_2^+$. The $\widetilde{B}^+$ $^2A_1$ and $\widetilde{C}^+$ $^2A_2$ photoelectron bands overlap in both $CH_2F_2^+$ and $CH_2Cl_2^+$, but they are 3 eV higher in energy than the ground-state band in $CH_2F_2^+$ whilst only 1 eV higher in $CH_2Cl_2^+$. When comparing the relative intensities of the bands under the three different recording conditions, the two obvious differences are that the intensity of the $\widetilde{X}^+/\widetilde{A}^+$ overlapped band compared to that of the $\widetilde{B}^+/\widetilde{C}^+$ band of CH_2Cl_2 is significantly reduced under threshold photoelectron conditions [29]. Second, under HeII photon conditions, the bands corresponding to ionisation from the $6b_2$, $8a_1$ and $2b_1$ orbitals ($\widetilde{D}^+$, $\widetilde{E}^+$ and $\widetilde{F}^+$) are much stronger compared to the four lower-energy bands [38].

The photoelectron spectrum of CH_2Cl_2 between 11.0 and 15.7 eV recorded with a resolution of *ca.* 0.003 eV is shown in Fig. 3 along with calculated adiabatic ionisation energies at the EOM-IP-CCSD/cc-pVTZ level of theory. An expansion of the ground-state band between 11.1 and 12.0 eV along with the FC simulation is shown in Fig. 4. This is the highest-resolution spectrum of this molecule reported in the literature so far. Our harmonic spectral simulations make it clear that there are two overlapping electronic band systems of the parent cation in this energy range. This is in agreement with Takeshita, who calculated the difference in vertical IE of the $\widetilde{X}^+$ $^2B_2$ and $\widetilde{A}^+$ $^2B_1$ states of $CH_2Cl_2^+$ to be only 0.04 eV [26]. However, the difference in adiabatic IE is calculated to be much greater, 0.41 eV, because ionisation to the $\widetilde{X}^+$ $^2B_2$ ground state involves a significant change in the ClCCl bond angle, whereas ionisation to $\widetilde{A}^+$ $^2B_1$ does not entail such a large change in any parameter. As stated in Section 1, harmonic calculations are more appropriate for $CH_2Cl_2^+$ than for $CH_2F_2^+$ because the lowest dissociation energy of the former cation corresponds not to H-atom but to Cl-atom loss, and occurs at 12.108 ± 0.003 eV which is *ca.* 1.3 eV (0.9 eV) above the predicted adiabatic IE of $\widetilde{X}^+$ $^2B_2$ ($\widetilde{A}^+$ $^2B_1$); the corresponding energy difference in $CH_2F_2^+$ is only 0.34 eV.

Our Franck–Condon calculations (details in Table S2 of Supplementary Material) show that vibrational activity in the $\widetilde{X}^+$ state is predicted to occur strongly in v_4^+ and weakly in v_3^+, modes which are CCl_2 bending and CCl_2 symmetric stretching vibrations, respectively. This is hardly surprising because of the 22° reduction in ClCCl bond angle upon ionisation from the $7b_2$ orbital of CH_2Cl_2 to yield the $\widetilde{X}^+$ state of the cation. The calculated maximum of this band of this band at 11.66 eV corresponds to $v_4^+ = 17$. The origin transition is thus derived to be located at 11.0 ± 0.2 eV with effectively zero FC factor, in excellent agreement with our

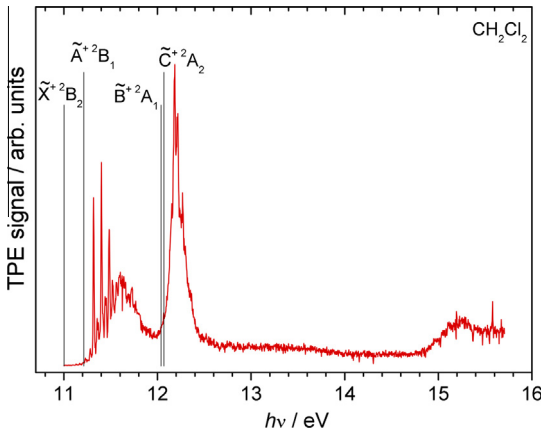

Fig. 3. The complete threshold photoelectron spectrum of CH_2Cl_2 in the 11.0–15.7 eV photon energy range recorded with a step size of 0.003 eV and an integration time of 25 s per point. The spectrum has been flux normalised. Vertical lines show adiabatic ionisation energies calculated at the EOM-IP-CCSD/cc-pVTZ level of theory.

calculated adiabatic ionisation energy of 11.01 eV. Hot band transitions originating from $v_4 = 1$ in the neutral to v_4^+ levels in the cation are also calculated to have significant intensity, and indeed for low v, the intensity of the 4_1^{v+1} band can be as strong as the nearly overlapping 4^v_0 band. There is also activity in combination bands involving v_4^+ with v_3^+. Although the relative geometry changes are smaller, the most significant change upon ionisation to the $\tilde{A}^+\ ^2B_1$ state of $CH_2Cl_2^+$ is a reduction of *ca.* 0.06 Å in the C–Cl bond length. It is therefore not surprising that the larger FC factors are calculated for transitions to the v_3^+ ladder (CCl_2 symmetric stretch), but peaking at the much lower level of $v_3^+ = 1$. In addition, combination bands of v_3^+ with v_4^+ also contribute to the experimental spectrum.

In attempting a complete spectral assignment of all the bands, it becomes quickly apparent that whilst the three strongest peaks at 11.317, 11.401 and 11.483 eV can easily be assigned to have their strongest component as $\tilde{A}^+\ ^2B_1\ 0_0^0$, 3_0^1 and 3_0^2 respectively, the picture for the remaining peaks is less clear. First, as is well known with long Franck–Condon progressions arising from a significant geometrical change between the two electronic states involved, the establishment of the absolute vibrational numbering in the unique progression observed (in this case, the $\tilde{X}^+\ 4^v_0$ and corresponding 4_1^{v+1} hot band) can be difficult to determine. Second, it is not clear how accurate *harmonic* Franck–Condon calculations

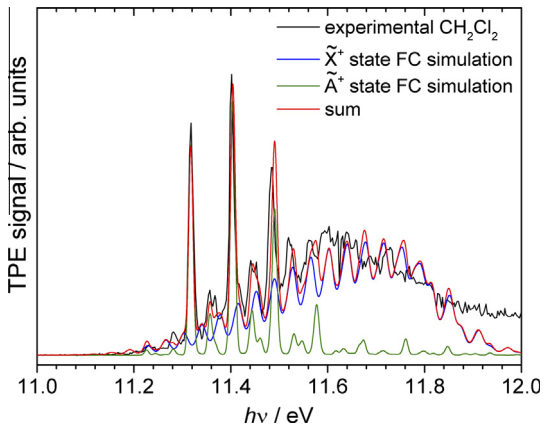

Fig. 4. An expansion of Fig. 3 between 11.1 and 12.0 eV. The first photoelectron band of CH_2Cl_2 consists of ionising transitions to the two overlapping states of $CH_2Cl_2^+$ $\tilde{X}^+\ ^2B_2$ and $\tilde{A}^+\ ^2B_1$. The vibrational structure based on a Franck-Condon simulation was calculated for both states. The sum of both simulations is also shown.

are for ionisation of CH_2Cl_2 to either the $\tilde{X}^+\ ^2B_2$ or $\tilde{A}^+\ ^2B_1$ states of the cation. In order to settle these issues, a PFI-ZEKE measurement of CH_2Cl_2 would be needed, similar to that reported for CH_2F_2 by Forysinski et al. [18], at a resolution an order of magnitude better than the TPES reported herein. With accompanying calculations such as reported in [19], this should then determine anharmonic effects on the vibrational energies and FC factors for ionisation of CH_2Cl_2 to ionic states which lie *ca.* 1.3 ($\tilde{X}^+\ ^2B_2$) and 0.9 ($\tilde{A}^+\ ^2B_1$) eV below the dissociation threshold to $CH_2Cl^+ + Cl + e^-$.

With these caveats stated, Fig. 4 shows a composite of the experimental threshold photoelectron spectrum of CH_2Cl_2 from 11.1 to 12.0 eV (black), simulations to the $\tilde{X}^+\ ^2B_2$ (blue) and $\tilde{A}^+\ ^2B_1$ (green) states of $CH_2Cl_2^+$, and simulation to the sum of both states (red). The agreement of experimental and theoretical spectrum is good. However, the simulation predicts a monotonously increasing intensity in the $\tilde{X}^+$ progression for four quanta longer than actually observed, probably due to anharmonic effects in the TPES. The calculated energies and intensities of the individual components and comparison with literature assignments are given in Table 4. Whilst most of the peaks with energies below 11.401 eV, the $\tilde{A}^+\ 3_0^1$ FC maximum, have a unique vibrational assignment involving one level of either $\tilde{X}^+$ or $\tilde{A}^+$, all peaks above this energy have a number of components, often from both ionic states, contributing to the blended assignment. This is a consequence of CH_2Cl_2 being a relatively heavy polyatomic molecule with several overlapping vibrational bands all allowed by the selection rules in photoelectron spectroscopy, quite apart from the additional problem of *two* ionic states being approximately degenerate. A comparison of our assignments with those of Pradeep and Shirley [37], Chim [29] and the early HeI study of Potts et al. [5] shows that we believe all of these earlier assignments are in parts incorrect; either it was not appreciated that there were two near-degenerate overlapping ionic states of $CH_2Cl_2^+$ [29], or that ionisation to $\tilde{X}^+\ ^2B_2$ involved such a large geometry change in the ClCCl bond angle that the v_4^+ progression would not start to gain significant FC factor until levels of v well above zero were accessed [5]. Pradeep and Shirley assign our $\tilde{A}^+$ progression to $^2B_2$ and the $\tilde{X}^+$ progression to the $^2B_1$ state, which implies their use of the *xz* convention just as they did in CH_2F_2. However, they refer to Takeshita's results, who used the *yz* convention, and cite a large ClCCl bond angle change in the $^2B_2$ state, which must be a misunderstanding. They also label the higher energy electronic states in the 15–17 eV range according to the *yz* convention also used herein. It is presumably because of this confusion that they could not appreciate Takeshita's prediction about the offset origin of the $\tilde{X}$ state and assume to see origin transitions for both lower lying states. Takeshita may also have contributed to this misunderstanding by using two different conventions on his treatise of CH_2F_2 and CH_2Cl_2 within a time span of a few months [15,26]. However, putting misunderstandings and absence of coordinate systems aside, an assignment of any spectrum can only relate to the resolution at which it is recorded, and the story of the last forty five years for the ground photoelectron band(s) of both CH_2F_2 and CH_2Cl_2 bears witness to this statement. We have no doubt that if and when this spectrum of CH_2Cl_2 is re-recorded with yet better resolution, new features will emerge, as happened with CH_2F_2 [18,19], and improved assignments will result.

3.3. Higher energy peaks in the valence photoelectron spectra of CH_2F_2 and CH_2Cl_2

3.3.1. Higher valence electronic states of $CH_2F_2^+$

The complete valence threshold photoelectron spectrum of CH_2F_2 at a resolution of *ca.* 0.006 eV is shown in Fig. 1. There are two major bands lying at higher energy to the ground-state band

Table 4
Energies (eV) of transitions observed in the vacuum-UV photoelectron bands of CH_2Cl_2 and comparison with earlier data.

$h\nu$ (eV)	Separation		Comment	FC simulation		Pradeep 1993[a]			Chim 2003[b]	
	(meV)	(cm^{-1})		$\widetilde{X}^+\,^2B_2$	$\widetilde{A}^+\,^2B_1$	$h\nu$	$\widetilde{X}^+\,^2B_2$	$\widetilde{A}^+\,^2B_1$	$h\nu$	Assignment
11.231	−86	−694	Hot band	$4_1^7/4_2^8$						
11.281	−36	−290	Hot band		4_1^0					
11.317	0	0	Adiabatic IE of $\widetilde{A}^+$		$0_0^0/4_1^1$	11.320	0_0^0		11.322	$\widetilde{X}^+/\widetilde{A}^{+*}\,0_0^0$
11.336	19	153	Shoulder	$4_0^9/4_1^{10}$						
11.357	40	323			$4_0^1/4_1^2$	11.357		0_0^0	11.364	$\widetilde{X}^+/\widetilde{A}^+\,2_0^1$
11.366	49	395		$4_0^{10}/4_1^{11}$						
11.401	84	677	Vertical IE of $\widetilde{A}^+$		$3_0^1/3_0^14_1^1$	11.404	3_0^1		11.408	$\widetilde{X}^+/\widetilde{A}^+\,3_0^1$
11.417	100	807	Shoulder	$4_0^{11}/4_1^{12}$		11.407		4_0^1		
11.442	125	1008		$4_0^{12}/4_1^{13}$	$3_0^14_0^1/3_0^14_1^2$	11.441		3_0^1	11.453	$\widetilde{X}^+/\widetilde{A}^+\,3_0^12_0^1$
11.454	137	1105			$3_0^24_1^0$	11.454		4_0^2		
11.483	166	1339		$4_0^{13}/4_1^{14}$	$3_0^2/3_0^24_1^1$	11.485	3_0^2		11.487	$\widetilde{X}^+/\widetilde{A}^+\,3_0^2$
11.504	187	1508	Weak							
11.522	205	1653	Broad	$4_0^{14}/4_1^{15}$	$3_0^24_0^1$	11.520		3_0^2	11.526	$\widetilde{X}^+/\widetilde{A}^+\,3_0^22_0^1$
11.540	223	1799	Weak		$2_0^13_0^1$					
11.563	246	1984		4_0^{15}	$3_0^3/3_0^34_1^1/3_0^27_0^2$	11.560	3_0^3			
11.597	280	2258	Broad	4_0^{16}		11.596		3_0^3		
11.640	323	2605	Vertical IE of $\widetilde{X}^+$	4_0^{17}		11.635	3_0^4			
11.657	340	2742		$3_0^14_0^{15}$		11.652		4_0^7 (?)		
11.688	371	2992	Weak, broad	4_0^{18}		11.666		3_0^4		
11.725	408	3291	Broad			11.690		4_0^8 (?)		
						11.729		4_0^9 (?)		
						11.731		3_0^5		

[a] Ref. [37]. The state symmetries are given as in the paper, the $\widetilde{X}^+$ and $\widetilde{A}^+$ progressions were misidentified and in fact correspond to the first excited and the ground electronic state of the cation, respectively. The convention used for the term symbols is unclear.
[b] Ref. [29].

already discussed in Section 3.1. They are (*i*) a broad peak from 14.5 to 16.5 eV with possible vibrational structure on the rising shoulder at lower energy and definite structure on the falling shoulder at high energy; and (*ii*) a peak from 18.5 to 20.0 eV with resolved structure in the low-energy rising edge. In addition, there appears to be a very weak and broad peak between 17 and 18 eV, not observed before, which may be due to autoionisation effects which are known to be prevalent in threshold photoelectron spectroscopy. We consider these two bands in turn.

3.3.1.1. 14.5–16.5 eV. Previous calculations predict that this peak encompasses the photoelectron bands arising from the overlap of electron removal from the (HOMO−*n*), *n* = 1, 2, and 3, orbitals, *i.e.* $\widetilde{A}^+\,^2B_2$, $\widetilde{B}^+\,^2A_1$ and $\widetilde{C}^+\,^2A_2$ [15,17,18]. Our spectrum has comparable signal to noise and resolution to that reported by Pradeep and Shirley [37], and our assignments and conclusions are quite similar. Within Koopmans' approximation these states arise from one-electron removal with no extensive configuration interaction [1]. Takeshita has calculated the geometries and reported harmonic vibrational frequencies of the a_1 symmetry normal modes for these three electronically excited states [15]. According to our calculations, for ionisation into $\widetilde{A}^+\,^2B_2$ state the most significant change in geometry is a reduction in the FCF angle from 108.6° to 83.8°, a similar effect to that predicted and observed for the ClCCl angle in the $CH_2Cl_2^+$ $\widetilde{X}^+\,^2B_2$ band (Section 3.2). Our spectrum in Fig. 5 shows partially-resolved steps in the rising edge of this broad band peaking at 15.34 eV. Pradeep and Shirley resolved these peaks slightly better, and reported an average vibrational spacing of 583 cm^{-1}, which they assigned to the CF_2 bending mode ν_4^+ [37]. It seems likely that the use of a supersonic beam and hence a low rotational temperature and narrow rotational envelope in the Pradeep and Shirley study means that the vibrational fine structure of the band is better resolved than in the room temperature spectrum in Fig. 5, even if our spectral resolution is better. The increase in the ν_4 frequency upon ionisation, the value in neutral CH_2F_2 being 528 cm^{-1} [11], is consistent with a reduction in FCF bond angle. Our Franck–Condon simulation of the $\widetilde{A}^+\,^2B_2$ state, also depicted in Fig. 5, shows a long progression in ν_4^+ with contributions from ν_2^+ and ν_3^+ always as combination bands with the ν_4^+ mode. The simulation nicely reproduces the step-like increase of the TPE signal at the rising edge of the band.

For electron removal from the $6a_1$ and $1a_2$ molecular orbitals producing $CH_2F_2^+$ $\widetilde{B}^+\,^2A_1$ and $\widetilde{C}^+\,^2A_2$, we calculated again significant changes in the FCF bond angle; +9.3° in $\widetilde{B}^+\,^2A_1$, and −11.2° in $\widetilde{C}^+\,^2A_2$, in good agreement with Takeshita's optimised geometries [15]. In addition, a 13.3° increase in HCH bond angle is predicted in $\widetilde{B}^+\,^2A_1$. While all other geometric changes are relatively small, the optimised C_{2v} symmetry $\widetilde{B}^+\,^2A_1$ structure was nevertheless found to be a transition state. Upon breaking symmetry, the ion relaxed into a C_S $[CH_2F^{+\cdots}F]$ A′ structure with three quasi-degenerate states corresponding to the three possible *p*-holes on the fluorine atom. Thus, the potential energy surface is unlikely to support bound C_{2v} $\widetilde{B}^+\,^2A_1$ states, and we do not expect any vibrational fine structure in the FC envelope of this state. On the high-energy part of this broad band, however, we observe two overlapping vibrational progressions (Fig. 1), which therefore appear to belong to the $\widetilde{C}^+\,^2A_2$ state. The main progression has peaks at 15.577, 15.704, 15.824, 15.948, 16.067 and 16.189 eV, with an average spacing of 988 cm^{-1}. A second progression with peaks at 15.632, 15.763, 15.881, 16.007 and 16.115 eV has a similar average spacing, and the peaks are displaced to higher energy by an average of 450 cm^{-1}. Pradeep and Shirley also observe these peaks and assign them to a ν_3^+ progression (CF_2 symmetric stretch, with some weak contribution from FCF bend), but they do not specify in which electronic state this progression is being observed [37].

The Franck–Condon simulation of this overlapped broad band supports the experimental findings. For the $\widetilde{C}^+\,^2A_2$ state, we determine an energy-minimum structure of r_e(C–H) = 1.083 Å, r_e

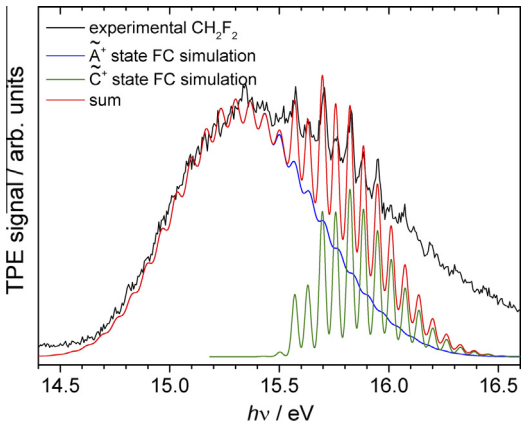

Fig. 5. The experimental spectrum of the second photoelectron band of CH_2F_2 between 14.5 and 16.5 eV, and simulation of the band assuming it is comprised of vibrational components of the $\widetilde{A}^+\ ^2B_2$ and $\widetilde{C}^+\ ^2A_2$ states. The spectrum fits remarkably well, despite the fact that the contributions of the $\widetilde{B}^+\ ^2A_1$ state were neglected.

(C–F) = 1.421 Å, ⟨HCH⟩ = 120.1°, ⟨FCF⟩ = 97.4° and ⟨HCF⟩ = 109.2°. The corresponding harmonic vibrational frequencies are also listed in Table 1. The low value of 646 cm^{-1} for ν_9^+ (CF_2 asymmetric stretch) is a consequence of the 0.07 Å increase in C–F bond length. The FC simulation predicts a progression in ν_3^+ peaking at $v = 1$, with each 3^n_0 peak having a combination peak with one quantum of ν_4^+ to higher energy. Our average spacing for ν_3^+ of 988 cm^{-1} can be compared with the harmonic calculation of 1027 cm^{-1}, our experimental value for ν_4^+ of 450 cm^{-1} is to be compared with the calculated value of 480 cm^{-1}. There are some weaker components involving two or four (*i.e.* even) quanta for ν_9^+ of b_2 symmetry, but they do not contribute significantly to the spectrum. Activity in ν_3^+ (CF_2 symmetric stretch), ν_4^+ (CF_2 bend) and ν_9^+ (CF_2 asymmetric stretch) is expected because of the 0.07 Å increase in C–F bond length and 11.2° decrease in FCF bond angle upon ionisation to this state. The combined simulation for the $\widetilde{A}^+$ and $\widetilde{C}^+$ states of $CH_2F_2^+$ is shown in Fig. 5, and details are given in Table S3 of the Supplementary Material. The simulation matches the experimental spectrum surprisingly well, notwithstanding any contributions from the repulsive $\widetilde{B}^+\ ^2A_1$ state. When comparing our results with those of Takeshita, we note that there is no mention of the $\widetilde{B}^+$ state being unbound as he carried out his calculations in C_{2v} symmetry. He also reported significantly higher values for ν_3^+ and ν_4^+ in the $\widetilde{C}^+\ ^2A_2$ state of $CH_2F_2^+$ of 1122 and 544 cm^{-1}, respectively [15]. Xi and Huang, on the other hand, reported a higher lying transition state (see later), but found that the $\widetilde{B}^+$ state was a minimum in C_{2v} [17]. By matching the simulated FC profiles to the experimental spectrum, we can now determine the adiabatic ionisation energies of the $\widetilde{A}^+$ and $\widetilde{C}^+$ states of CH_2F_2 to be 14.3 ± 0.1 and 15.57 ± 0.01 eV. While the $\widetilde{C}^+$ state can be clearly identified from the spectrum, the origin of $\widetilde{A}^+$ can only be extrapolated by shifting the whole FC envelope to fit the band, resulting in a larger error bar of at least one vibrational quantum in ν_4^+.

In summary, we agree with the assignment for this band of Pradeep and Shirley [37], but believe that the discrete structure on the high-energy shoulder is due to intensity in ν_3^+ in combination bands with ν_4^+ in the $\widetilde{C}^+\ ^2A_2$ state, not a combination of activity in both $\widetilde{B}^+\ ^2A_1$ and $\widetilde{C}^+\ ^2A_2$ states. The low-energy part of the band can be assigned by FC simulation to vibrational activity in ν_4^+ in the $\widetilde{A}^+\ ^2B_2$ band.

3.3.1.2. 18.5–20.0 eV. This band (Fig. 6) comprises three overlapping electronic states of $CH_2F_2^+$; $\widetilde{D}^+\ ^2B_2$, $\widetilde{E}^+\ ^2A_1$ and $\widetilde{F}^+\ ^2B_1$. The $3b_2$, $5a_1$ and $1b_1$ orbitals of CH_2F_2 are essentially near-degenerate C–F bonding orbitals [6]. As seen by earlier HeI studies, we also observe a single progression, with energies of partially resolved peaks at 18.296, 18.377, 18.462, 18.546, 18.627, 18.712, 18.792, and 18.877 eV. The maximum of the overlapped band is at 18.98 eV. This average spacing of 0.083 eV or 670 cm^{-1} agrees with the spacing observed by Potts et al. [5]. Brundle et al. measure a slightly lower value of 645 cm^{-1} [6]. Pradeep and Shirley claim to partially resolve three overlapping progressions, corresponding to the CF_2 symmetric stretching mode ν_3^+ in each of the near-degenerate $\widetilde{D}^+$ (724 cm^{-1}), $\widetilde{E}^+$ (673 cm^{-1}) and $\widetilde{F}^+$ (727 cm^{-1}) states [37], but the signal-to-noise ratio of their published spectrum hardly justifies such an optimistic assignment. However, all studies agree that the significant reduction in the vibrational energy of this ν_3 mode from its value in neutral CH_2F_2, 1112 cm^{-1} [10], is consistent with electron removal from C–F bonding orbitals. We succeeded in optimising the geometries of these states at the EOM-IP-CCSD/cc-pVTZ level of theory. However, only the $\widetilde{D}^+$ state is a true minimum on the potential energy surface. The $\widetilde{E}^+$ and $\widetilde{F}^+$ states possess imaginary frequencies in the CF asymmetric stretch and CH_2 twist mode, respectively, and it was not possible to locate further minima other than the $\widetilde{D}^+$ state by breaking the symmetry and letting the geometry relax. This is at odds with the results of Xi and Huang, who found $\widetilde{D}^+\ ^2B_2$ to be a transition state and the $^2A_1$ state to be a minimum [17]. A FC simulation predicts the vibrational progression on the low-energy side of the band very well, with dominant contributions from the CF_2 stretch (ν_3^+) and FCF bend (ν_4^+) modes of the $\widetilde{D}^+$ state and their combination bands. Based on the simulation, details for which are given in Table S4 of the Supplementary Material, we can determine the adiabatic ionisation energy to the $\widetilde{D}^+\ ^2B_2$ state to be 18.0 ± 0.1 eV.

3.3.2. Higher valence electronic states of $CH_2Cl_2^+$

The second photoelectron band of CH_2Cl_2 between 12.0 and 12.5 eV corresponds to ionisation from the $9a_1$ and the $2a_2$ molecular orbitals, which are essentially associated with the chlorine *p* lone pair orbitals perpendicular ($9a_1$, $2p\pi$ bonding character) and parallel to the principal Cl–C–Cl plane ($2a_2$, $2p\pi$ non-bonding character) [39]. Removing an electron from the $9a_1$ orbital with π bonding character between the chlorine atoms leads to an increase in the Cl–C–Cl bond angle of 8.5° (Table 2). The Franck–Condon simulation of the $\widetilde{B}^+\ ^2A_1$ state (Fig. 7, green) exhibits clear vibrational activity in the CCl_2 bending mode (ν_4^+) with minor contributions from combinations bands with ν_3^+ (CCl_2 symmetric stretch) and ν_2^+ (CH_2 bend). The spectral feature at around 12.1 eV of the experimental spectrum is associated with a hot band in ν_4 which is significantly populated at room temperature, while the shoulder at 12.15 eV can be assigned to the 0–0 transition. However, the experimental band cannot be reproduced by vibrational contributions from the $\widetilde{B}^+\ ^2A_1$ state alone. According to our EOM-IP-CCSD calculations (Fig. 3) the $\widetilde{B}^+\ ^2A_1$ and $\widetilde{C}^+\ ^2A_2$ states are almost degenerate, as was also reported by Takeshita [26]. Ionisation from the $2a_2$ orbital, having antibonding character between the chlorine ligands, results in a decrease of the Cl–C–Cl angle of 7.6° (Table 2) and thus activity in ν_4^+ also upon ionisation (Fig. 7, blue). Minor contributions from the ν_3^+ mode are also visible in the stick spectrum but are blended out in the convolution with a Gaussian function with a FWHM of 27 meV. At 12.2 eV, a hot band in ν_4 contributes to the simulated spectrum, which is followed by the 0–0 transition at 12.25 eV. The sum of both simulated spectra (details for which are given in Table S5 of the Supplementary Material) reproduces the overall shape of the second photoelectron band of CH_2Cl_2 extremely well. Based on the features of the

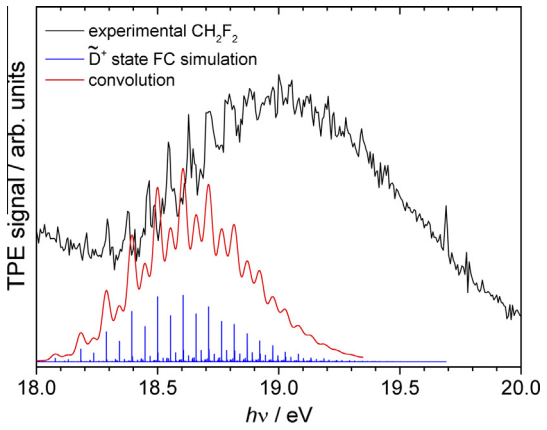

Fig. 6. The experimental spectrum of the third photoelectron band of CH_2F_2 between 18 and 20 eV, and Franck Condon simulation of the $\tilde{D}^+ {}^2B_2$ state.

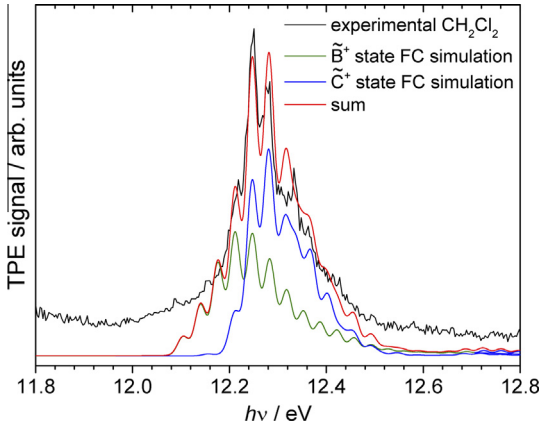

Fig. 7. The experimental spectrum of the third photoelectron band of CH_2Cl_2 (black), ionisation to $\tilde{B}^+ {}^2A_1$ (green) and $\tilde{C}^+ {}^2A_2$ (blue), and simulations of the Franck Condon vibrational components, calculated in the harmonic approximation (see Section 3.3.2). The red curve, the sum of both calculations, is in good agreement with the experimental spectrum.

experimental spectrum and the simulations, we determine the adiabatic ionisation energies for these two ion states to be 12.15 and 12.25 eV.

The spectrum of Pradeep and Shirley [37] is very similar in signal-to-noise ratio and resolution to ours of Fig. 7. They assign the partially resolved peaks to vibrational progressions in ν_4^+ in both of these ionic states, in agreement with our findings. Our calculations for the $\tilde{C}^+ {}^2A_2$ state also show that Franck–Condon intensity in ν_3^+ is comparable to that in ν_4^+ at around 12.33 eV, leading to significant broadening of the spectral features. As noted earlier, a PFI-ZEKE spectrum of a rovibrationally cold sample recorded at *ca.* 1 cm^{-1} or better resolution would be needed to take this analysis further. The next band with an onset at *ca.* 15 eV (Fig. 3) corresponds to ionisation to three overlapping states of $CH_2Cl_2^+$; $\tilde{D}^+ {}^2B_2$, $\tilde{E}^+ {}^2A_1$ and $\tilde{F}^+ {}^2B_1$. This is the equivalent band to that in CH_2F_2 between 18.5 and 20.0 eV (Section 3.3.1), but here we were not able to resolve vibrational structure.

4. Conclusions

Using the imaging photoelectron photoion coincidence spectrometer at the VUV beamline of the 3rd generation Swiss Light Source, we have recorded the threshold photoelectron spectrum of CH_2F_2 and CH_2Cl_2 from threshold up to *ca.* 20 eV at a resolution of up to 2 meV or 16 cm^{-1}. With the help of (EOM-IP-)CCSD calculations and Franck–Condon simulations, we were able to model the observed vibrational fine structure of the ground and excited ion states. For CH_2F_2 we determine an adiabatic (vertical) ionisation energy of 12.727 ± 0.004 (13.158 ± 0.004) eV. FC modelling only delivered a qualitative but not a quantitative fit to the barely-bound ground state of the $CH_2F_2^+$ cation, pointing to the importance of the effects of anharmonicity close to dissociation barriers, as discussed in detail by Luckhaus et al. [19]. The CH_2F_2 photoelectron band between 14.5 and 16.5 eV encompasses ionisation to three overlapping states of the cation, $\tilde{A}^+ {}^2B_2$, $\tilde{B}^+ {}^2A_1$ and $\tilde{C}^+ {}^2A_2$. Applying EOM-IP-CCSD calculations, we were able to find C_{2v} equilibrium structures of two of the three states, to carry out a Franck–Condon simulation of the observed vibrational progressions, and derive adiabatic (vertical) ionisation energies of 14.3 ± 0.1 (15.18 ± 0.07) and 15.57 ± 0.01 (15.73 ± 0.02) eV for the $\tilde{A}^+ {}^2B_2$ and $\tilde{C}^+ {}^2A_2$ states, respectively. The $\tilde{B}^+ {}^2A_1$ state was found to relax to a C_S symmetry $[CH_2F^{+\cdots}F]$ structure and is considered to be repulsive in its FC envelope. In a third band, we were able to fit a single vibrational progression to derive an adiabatic (vertical) ionisation energy to the $\tilde{D}^+ {}^2B_2$ state of 18.0 ± 0.1 (18.58 ± 0.05) eV.

The first photoelectron band of CH_2Cl_2 has two overlapping components, namely ionisation to the $\tilde{X}^+ {}^2B_2$ and $\tilde{A}^+ {}^2B_1$ states. The first ionic state shows an extended progression in ν_4^+ (CCl_2 bend) arising from a large decrease in ClCCl bond angle upon ionisation, while the first excited state has a much shorter progression in ν_3^+ (CCl_2 symmetric stretch) with intensity condensed into $v = 0$–2. A simultaneous Franck–Condon modelling of the two states yielded adiabatic (vertical) ionisation energies of 11.0 ± 0.2 (11.64 ± 0.08) and 11.317 ± 0.006 (11.404 ± 0.006) eV for the $\tilde{X}^+$ and $\tilde{A}^+$ states, respectively. The second photoelectron band between 12.0 and 12.5 eV is also comprised of two states exhibiting vibrational structure, $\tilde{B}^+ {}^2A_1$ and $\tilde{C}^+ {}^2A_2$, with derived adiabatic (vertical) ionisation energies of 12.15 ± 0.02 (12.221 ± 0.008) and 12.25 ± 0.02 (12.284 ± 0.008) eV, respectively.

When we compared our spectra and assignments with the literature, it became evident how crucial it is to provide the auxiliary information necessary to interpret term symbols and symmetries. There is no single accepted way of orienting C_{2v} symmetry molecules in space, which means that the B_1 and B_2 representations are only defined if the principal plane of the molecule is specified. In some papers, this was done. Sometimes, it was possible to deduce the convention used based on, for example, orbital ordering even when the principal plane was not given. However, in the more complicated case of CH_2Cl_2 in which the first observed transition belongs to the first *excited* $\tilde{A}^+$ state which is a result of ionisation from the HOMO, and not the (HOMO−1) orbital, deducing the convention(s) used can prove to be an insurmountable obstacle to even the most intrepid molecular spectroscopist. In this work, we chose *yz* as the principal plane.

As both experimental and theoretical methods have improved over the last four decades, so has our understanding of the photoelectron spectrum of these two medium-sized molecules. The spectrum of the first band of CH_2F_2, ionisation to $\tilde{X}^+ {}^2B_1$, has now been recorded at sub-wavenumber resolution by PFI-ZEKE spectroscopy [18], and further work on the overlapping $\tilde{X}^+ {}^2B_2$ and $\tilde{A}^+ {}^2B_1$ bands in the spectrum of CH_2Cl_2 can only progress with the improvement in resolution that this laser-based technique brings. However, as shown here, even smaller improvements in spectral resolution can yield deeper insights into the assignment of the transitions, particularly in conjunction with modelling the spectra with computational chemistry methods.

Acknowledgments

Experiments were carried out at the VUV beamline of the Swiss Light Source at the Paul Scherrer Institute, with funding from the European Community's Seventh Framework Programme (FP7/2007-2013) under grant agreement no. 226716. Dr Nicola Rogers (University of Durham, UK) took part in recording the spectra and we thank Professor Tom Baer (University of North Carolina, USA) for discussions on forbidden transitions in threshold photoelectron spectroscopy. JH thanks the University of Birmingham for a Research Studentship. AB and PH acknowledge funding by the Swiss Federal Office for Energy (BFE Contract 101969/152433).

Appendix A. Supplementary material

Supplementary data associated with this article can be found, in the online version, at http://dx.doi.org/10.1016/j.jms.2015.02.012.

References

[1] T. Koopmans, Physica 1 (1934) 104.
[2] D. Sprecher, C. Jungen, W. Ubachs, F. Merkt, Faraday Discuss. 150 (2011) 51.
[3] O.V. Boyarkin, M.A. Koshelev, O. Aseev, P. Maksyutenko, T.R. Rizzo, N.F. Zobov, L. Lodi, J. Tennyson, O.L. Polyansky, Chem. Phys. Lett. 568–569 (2013) 14.
[4] T. Baer, B. Sztaray, J.P. Kercher, A.F. Lago, A. Bodi, C. Skull, D. Palathinkal, Phys. Chem. Chem. Phys. 7 (2005) 1507.
[5] A.W. Potts, H.J. Lempka, D.G. Streets, W.C. Price, Philos. Trans. R. Soc. A Math. Phys. Eng. Sci. 268 (1970) 59.
[6] C.R. Brundle, M.B. Robin, H. Basch, J. Chem. Phys. 53 (1970) 2196.
[7] B.P. Pullen, T.A. Carlson, W.E. Moddeman, G.K. Schweitzer, W.E. Bull, F.A. Grimm, J. Chem. Phys. 53 (1970) 768.
[8] E. Hirota, J. Mol. Spectrosc. 71 (1978) 145.
[9] J.L. Duncan, J. Mol. Struct. 158 (1987) 169.
[10] K.M. Smith, G. Duxbury, D.A. Newnham, J. Ballard, J. Mol. Spectrosc. 193 (1999) 166.
[11] K.M. Smith, D.A. Newnham, M. Page, J. Ballard, G. Duxbury, J. Quant. Spectrosc. Radiat. Transf. 56 (1996) 73.
[12] M.N. Deo, R. D'Cunha, V.A. Job, J. Mol. Spectrosc. 161 (1993) 403.
[13] M.N. Deo, K. Kawaguchi, R. D'Cunha, J. Mol. Struct. 517–518 (2000) 187.
[14] T.J. Cronin, X. Wang, G.A. Bethardy, D.S. Perry, J. Mol. Spectrosc. 194 (1999) 236.
[15] K. Takeshita, Chem. Phys. Lett. 165 (1990) 232.
[16] R.D. Amos, N.C. Handy, W.H. Green, D. Jayatilaka, A. Willetts, P. Palmieri, J. Chem. Phys. 95 (1991) 8323.
[17] H.W. Xi, M.B. Huang, Chem. Phys. Lett. 430 (2006) 227.
[18] P.W. Forysinski, P. Zielke, D. Luckhaus, R. Signorell, Phys. Chem. Chem. Phys. 12 (2010) 3121.
[19] D. Luckhaus, P.W. Forysinski, P. Zielke, R. Signorell, Mol. Phys. 108 (2010) 2325.
[20] J. Harvey, R.P. Tuckett, A. Bodi, J. Phys. Chem. A 116 (2012) 9696.
[21] M. Snels, J. Mol. Spectrosc. 183 (1997) 224.
[22] J.L. Duncan, G.D. Nivellini, F. Tullini, J. Mol. Spectrosc. 118 (1986) 145.
[23] F. Tullini, M. Dinelli, G.D. Nivellini, J.L. Duncan, Spectrochim. Acta Part A Mol. Spectrosc. 42 (1986) 1165.
[24] A. Morone, M. Snels, O. Polanz, J. Mol. Spectrosc. 173 (1995) 113.
[25] R. Escribano, J.M. Orza, S. Montero, C. Domingo, Mol. Phys. 37 (1979) 361.
[26] K. Takeshita, Chem. Phys. 143 (1990) 239.
[27] A.F. Lago, J.P. Kercher, A. Bödi, B. Sztáray, B. Miller, D. Wurzelmann, T. Baer, J. Phys. Chem. A 109 (2005) 1802.
[28] D.P. Seccombe, R.P. Tuckett, B.O. Fisher, J. Chem. Phys. 114 (2001) 4074.
[29] R.Y.L. Chim, Ph.D. Thesis, University of Birmingham, 2003. <http://etheses.bham.ac.uk/1526/>.
[30] A. Bodi, M. Johnson, T. Gerber, Z. Gengeliczki, B. Sztaray, T. Baer, Rev. Sci. Instrum. 80 (2009) 34101.
[31] A. Bodi, P. Hemberger, T. Gerber, B. Sztáray, Rev. Sci. Instrum. 83 (2012) 083105.
[32] B. Sztaray, T. Baer, Rev. Sci. Instrum. 74 (2003) 3763.
[33] J. Harvey, P. Hemberger, A. Bodi, R.P. Tuckett, J. Chem. Phys. 138 (2013) 124301.
[34] A. Bodi, N.S. Shuman, T. Baer, Phys. Chem. Chem. Phys. 11 (2009) 11013.
[35] Y. Shao, L.F. Molnar, Y. Jung, J. Kussmann, C. Ochsenfeld, S.T. Brown, A.T.B. Gilbert, L. V Slipchenko, S. V Levchenko, D.P. O'Neill, R.A. DiStasio, R.C. Lochan, T. Wang, G.J.O. Beran, N.A. Besley, J.M. Herbert, C.Y. Lin, T. Van Voorhis, S.H. Chien, A. Sodt, R.P. Steele, V.A. Rassolov, P.E. Maslen, P.P. Korambath, R.D. Adamson, B. Austin, J. Baker, E.F.C. Byrd, H. Dachsel, R.J. Doerksen, A. Dreuw, B.D. Dunietz, A.D. Dutoi, T.R. Furlani, S.R. Gwaltney, A. Heyden, S. Hirata, C.-P. Hsu, G. Kedziora, R.Z. Khalliulin, P. Klunzinger, A.M. Lee, M.S. Lee, W. Liang, I. Lotan, N. Nair, B. Peters, E.I. Proynov, P.A. Pieniazek, Y.M. Rhee, J. Ritchie, E. Rosta, C.D. Sherrill, A.C. Simmonett, J.E. Subotnik, H.L. Woodcock, W. Zhang, A.T. Bell, A.K. Chakraborty, D.M. Chipman, F.J. Keil, A. Warshel, W.J. Hehre, H.F. Schaefer, J. Kong, A.I. Krylov, P.M.W. Gill, M. Head-Gordon, Phys. Chem. Chem. Phys. 8 (2006) 3172.
[36] V.A. Mozhayskiy, A.I. Krylov, ezSpectrum, <http://iopenshell.usc.edu/downloads>.
[37] T. Pradeep, D.A. Shirley, J. Electron Spectros. Relat. Phenomena 66 (1993) 125.
[38] W. von Niessen, L. Åsbrink, G. Bieri, L. Asbrink, W. von Niessen, L. Asbrink, J. Electron Spectrosc. Relat. Phenomena 26 (1982) 173.
[39] R.N. Dixon, J.N. Murrell, B. Narayan, Mol. Phys. 20 (1971) 611.
[40] H.W. Xi, M.B. Huang, Chem. Phys. Lett. 425 (2006) 28.